Supplementary Information for: "Interplay between disorder and topology in Thouless pumping on a superconducting quantum processor"

Yu Liu,[1,2,*] Yu-Ran Zhang,[3,*] Yun-Hao Shi,[1,2,4] Tao Liu,[3] Congwei Lu,[5] Yong-Yi Wang,[1,2] Hao Li,[1] Tian-Ming Li,[1,2] Cheng-Lin Deng,[1,2] Si-Yun Zhou,[1,2] Tong Liu,[1] Jia-Chi Zhang,[1,2] Gui-Han Liang,[1,2] Zheng-Yang Mei,[1,2] Wei-Guo Ma,[1,2] Hao-Tian Liu,[1,2] Zheng-He Liu,[1,2] Chi-Tong Chen,[1,2] Kaixuan Huang,[4] Xiaohui Song,[1] S. P. Zhao,[1,2,6] Ye Tian,[1] Zhongcheng Xiang,[1,2,7,†] Dongning Zheng,[1,2,6,7,8] Franco Nori,[9,10,11] Kai Xu,[1,2,4,6,7,8,‡] and Heng Fan[1,2,4,6,7,8,§]

[1]*Institute of Physics, Chinese Academy of Sciences, Beijing 100190, China*
[2]*School of Physical Sciences, University of Chinese Academy of Sciences, Beijing 100049, China*
[3]*School of Physics and Optoelectronics, South China University of Technology, Guangzhou 510640, China*
[4]*Beijing Academy of Quantum Information Sciences, Beijing 100193, China*
[5]*Department of Physics, Applied Optics Beijing Normal University, Beijing 100875, China*
[6]*Songshan Lake Materials Laboratory, Dongguan, Guangdong 523808, China*
[7]*Hefei National Laboratory, Hefei 230088, China*
[8]*CAS Center for Excellence in Topological Quantum Computation, UCAS, Beijing 100049, China*
[9]*Theoretical Quantum Physics Laboratory, Cluster for Pioneering Research, RIKEN, Wako-shi, Saitama 351-0198, Japan*
[10]*Center for Quantum Computing, RIKEN, Wako-shi, Saitama 351-0198, Japan*
[11]*Physics Department, University of Michigan, Ann Arbor, Michigan 48109-1040, USA*

Contents

* These authors contributed equally to this work.
† zcxiang@iphy.ac.cn
‡ kaixu@iphy.ac.cn
§ hfan@iphy.ac.cn

Supplementary Note I: Experimental setup

Our experiments are performed on *Chuang-tzu*, a 1D superconducting processor, containing 43 transmon qubits, which is the same processor used in [1]. The qubits are designed to be frequency-tunable with a mean sweet point of about $5.8\,\mathrm{GHz}$, and each qubit is capacitively coupled to its nearby qubits with a mean coupling strength of about $7.2\,\mathrm{MHz}$. We use 41 qubits, i.e., Q_1–Q_{41}, in our experiments, and all relevant information about qubit characteristics is listed in Supplementary Table 1. All qubits are initialized at their idle frequencies distributing over the range from $4.4\,\mathrm{GHz}$ to $5.6\,\mathrm{GHz}$, which are carefully arranged to minimize the unexpected interaction and crosstalk errors. The anharmonicity, $\alpha_j/2\pi$, of qubits is about $0.2\,\mathrm{GHz}$, and the qubit working frequency is adjusted to be $4.8\,\mathrm{GHz}$. We tune all qubit frequencies and coupling strengths to the target points by applying the automatic calibration scheme as mentioned in Ref. [1].

Supplementary Note II: Model and Hamiltonian

A. Pumping, polarization, and topology

One simple manifestation of topology in quantum systems is Thouless pumping, entailing quantized transport through an adiabatic cyclic evolution of a 1D quantum system in the absence of the net electromagnetic field [2–4]. The physics and topological nature of pumping can be demonstrated by periodically modulating the Rice-Mele (RM) model [5] written as:

$$\hat{H}_{\mathrm{RM}} = \sum_{j=0}^{L-2}[J + (-1)^j\delta](\hat{a}_j^\dagger\hat{a}_{j+1} + \mathrm{H.c.}) + \sum_{j=0}^{L-1}(-1)^j\Delta\hat{a}_j^\dagger\hat{a}_j, \tag{1}$$

where $\hat{a}^\dagger(\hat{a})$ denotes the creation (annihilation) operator, the chain length $L = 2N$ is even, $\pm\Delta$ are staggered on-site potentials, and $J \pm \delta$ are alternating hopping strengths. When $\Delta/2\pi = 0$ MHz, the RM model in Supplementary Eq. (1) reduces to the celebrated Su-Shrieffer-Heeger (SSH) model [6]. Under periodic boundary conditions (PBC), the energy spectrum of $\hat{H}_{\mathrm{RM}}$ consists of two bands, separated by a gap except a gapless point at $(\Delta/2\pi, \delta/2\pi) = (0\ \mathrm{MHz}, 0\ \mathrm{MHz})$.

Parameter	Mean	Median	Stdev.	Units
Qubit maximum frequency $\omega_{\mathrm{m}}/2\pi$	5.83	5.768	0.289	GHz
Qubit idle frequency $\omega_{\mathrm{i}}/2\pi$	5.014	4.777	0.428	GHz
Qubit anharmonicity $\alpha_j/2\pi$	-0.208	-0.193	0.02	GHz
Readout frequency $\omega_{\mathrm{r}}/2\pi$	6.68	6.684	0.052	GHz
Mean energy relaxation time $\overline{T}_1$	21.0	20.9	6.0	μs
Pure dephasing time at idle frequency T_2^*	0.826	0.759	0.25	μs
Qubit-Qubit coupling $g_{j,j+1}/2\pi$	7.11	7.20	0.39	MHz
Qubit-resonator coupling $g_{\mathrm{qr}}/2\pi$	36.62	38.15	35.26	MHz
Mean fidelity of single-qubit gates	99.2	99.4	1.1	%

Supplementary Table 1. Device parameters.

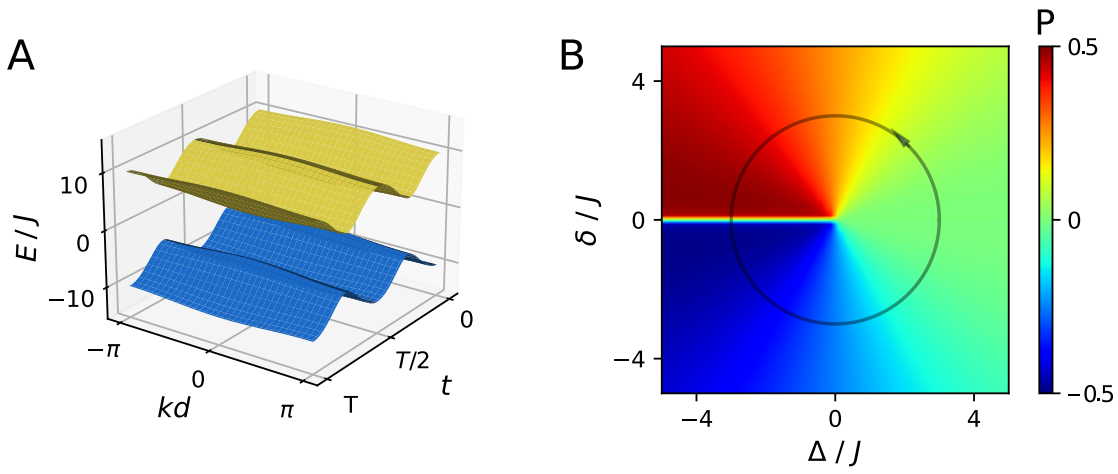

Supplementary Fig. 1. Energy bands of the Rice-Mele model and the polarization P. (**A**) The band structure in the k-t Brillouin zone under PBC, containing two bands separated by a gap. (**B**) Polarization P in a unit of the lattice constant ($d = 2$) versus the Rice-Mele model parameters Δ and δ. The discontinuity is due to the particular choice of the eigenstate phase.

With PBC and periodic driving, we could define the Bloch wavefunction of the n-th band in a k-t Brillouin zone as $|\psi_{k,n}\rangle = e^{ikx}\,|u_{n,k}\rangle$, due to the periodicity of the lattice in both space and time. The band structure is plotted in Supplementary Fig. 1A. When Δ and δ vary adiabatically with a sufficiently slow period T and the n-th band is evenly filled, we can define the Chern number as

$$\nu_n = \frac{1}{2\pi}\int_0^T \mathrm{d}t \int_{1\mathrm{BZ}} \mathrm{d}k\ \Omega_n(k,t), \tag{2}$$

where $\Omega_n(k,t) \equiv \mathrm{i}(\langle\partial_t u_{n,k}|\,\partial_k u_{n,k}\rangle - \langle\partial_k u_{n,k}|\,\partial_t u_{n,t}\rangle)$ is the Berry curvature, and 1BZ denotes the first Brillouin zone. The integer Chern number characterizes quantized charge transport in the adiabatic limit, and the pumped amount of charge over one cycle ΔQ can be expressed as

$$\Delta Q = d\int_0^T \mathrm{d}t\ \langle\psi(t)|\,\hat{\mathcal{J}}(t)\,|\psi(t)\rangle\,, \tag{3}$$

where $d = 2$ is the lattice constant because of the staggered parameters. Here,

$$\hat{\mathcal{J}}(t) = \frac{\mathrm{i}}{L}\sum_{j=1}^{L}(J + (-1)^j\delta)\hat{a}_{j+1}^\dagger\hat{a}_j + \mathrm{H.c.} \tag{4}$$

denotes the average current density [7, 8], and $|\psi(t)\rangle$ is obtained by evolving the N-particle ground state $|\psi(0)\rangle$.

By performing a Fourier transformation (FT) on the Bloch state, we can introduce the Wannier state localized at site j for the n-th Bloch band as

$$|w_{n,j}\rangle = \frac{1}{\sqrt{N}}\sum_k \mathrm{e}^{-\mathrm{i}jk}\,|\psi_{n,k}\rangle\,. \tag{5}$$

The position matrix elements of the Wannier states in the thermodynamic limit ($N \to \infty$) can be calculated as

$$\begin{aligned}
\mathsf{P} - j = \langle w_{n,j}| \hat{x} - j |w_{n,j}\rangle =& \frac{1}{N}\sum_{k,k'} \langle u_{n,k'}| \, \mathrm{e}^{-\mathrm{i}k'(x-j)}(x-j)\mathrm{e}^{\mathrm{i}k(x-j)} \, |u_{n,k}\rangle \\
=& \frac{d^2}{4\pi^2}\int \mathrm{d}x \int \mathrm{d}k\mathrm{d}k' \; u^*_{n,k'}(x,t)\mathrm{e}^{-\mathrm{i}k'(x-j)}[-\mathrm{i}\partial_k \mathrm{e}^{\mathrm{i}k(x-j)}]u_{n,k}(x,t) \\
=& \frac{d}{2\pi}\int_{1\mathrm{BZ}} \mathrm{d}k \; \langle u_{n,k}| \, \mathrm{i}\partial_k u_{n,k}\rangle \\
=& \frac{d}{2\pi}\int_{1\mathrm{BZ}} \mathrm{d}k \; \mathcal{A}^k_n(k,t),
\end{aligned} \tag{6}$$

where $\mathcal{A}^k_n(k,t)$ is the Berry connection, and $\mathsf{P} = \langle w_{n,j}| \, \hat{x} \, |w_{n,j}\rangle$ denotes the polarization [9] as a quantum extension of the classical electric polarization. When the initial state is prepared as a Wannier state $|w_{n,j}\rangle$, the change of the polarization over one cycle is given by

$$\begin{aligned}
\Delta\mathsf{P} =& \frac{d}{2\pi}\int_0^T \mathrm{d}t \int_{1\mathrm{BZ}} \mathrm{d}k \; \partial_t \mathcal{A}^k_n(k,t) \\
=& \frac{d}{2\pi}\int_0^T \mathrm{d}t \int_{1\mathrm{BZ}} \mathrm{d}k \; (\mathrm{i}\partial_t \langle u_{n,k}| \, \partial_k u_{n,k}\rangle - \mathrm{i}\partial_k \langle u_{n,k}| \, \partial_t u_{n,k}\rangle) \\
=& \nu_n d,
\end{aligned} \tag{7}$$

which can also be obtained by calculating the change of P for a parameter pair (Δ, δ), as shown in Supplementary Fig. 1B. The change of P is connected to the number of the evolving trajectory in Δ-δ space, winding the gapless point $(0,0)$.

B. Maximally localized Wannier state

Due to the gauge freedom of Bloch functions, the Wannier state defined in Supplementary Eq. (5) is non-unique [10]. More specifically, if we replace $|\psi_{n,k}\rangle$ to $|\tilde{\psi}_{n,k}\rangle = \mathrm{e}^{\mathrm{i}\varphi_n(k)}|\psi_{n,k}\rangle$, with $\varphi_n(k)$ being smooth real functions that is periodic in the momentum space, different sets of Wannier states will be defined, having distinct shapes and spreads. By introducing the second order moment of the position operator of $|w_{n,0}\rangle$

$$\Omega = \sum_n \left[\langle w_{n,0}| \, \hat{x}^2 \, |w_{n,0}\rangle - \langle w_{n,0}| \, \hat{x} \, |w_{n,0}\rangle^2\right] \tag{8}$$

as the localization criterion, Marzari and Vanderbilt developed an effective approach to constrain the freedom gauge [11]. Through minimizing Ω, we can obtain the maximally localized Wannier state (MLWS).

For 1D quantum systems, MLWS can be calculated as the eigenstates of the projected position operator in the real space, $\hat{P}\hat{x}\hat{P}$, with $\hat{P} = \sum_k |\psi_{n,k}\rangle \langle\psi_{n,k}|$ the projection operator to a filled band. However, the usual definition of $\hat{x}$ is vague when crossing the boundary under PBC. Alternatively, $\hat{x}$ can be substituted to a unitary operator $\hat{X} = \mathrm{e}^{\mathrm{i}\frac{2\pi}{N}\hat{x}}$, and the task to solve MLWS is transformed into diagonalization of

$$\hat{X}_P = \hat{P}\hat{X}\hat{P}. \tag{9}$$

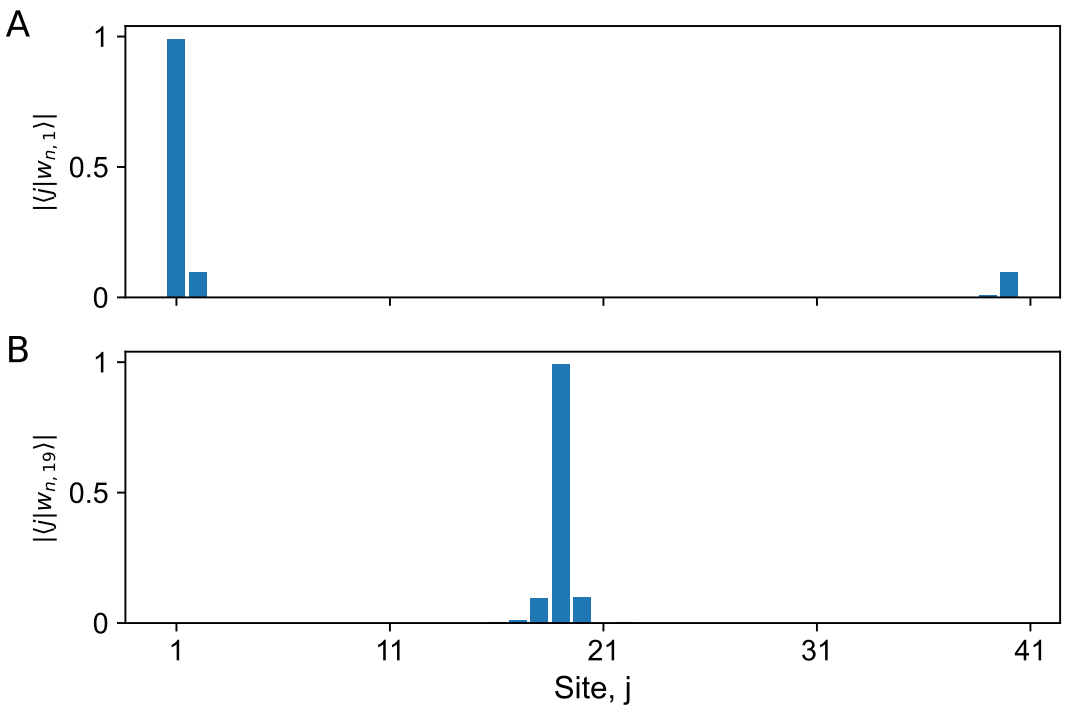

Supplementary Fig. 2. The wavefunctions of maximally localized Wannier state localized at the edge (**A**) and the center (**B**) of the Rice-Mele model with $N = 20$.

Note that in general $\hat{X}_P$ is not Hermitian, meaning that the eigenstates are not orthogonal except for the thermodynamic limit.

Numerically, we calculate MLWS of the RM model for each energy band based on the experimental setup. Two typical wavefunctions of MLWS localized at the edge and center individually are shown in Supplementary Fig. 2. We find that a single particle localized at site j approximates a Wannier state of a half-filling (upper or lower) band that is determined by the parity of the site [12]. The quantum state fidelity between a single-particle excitation and the corresponding MLWS is larger than 0.99.

Thus, quantized transport, indicated by the Chern number, can be observed experimentally by measuring the displacement of the center-of-mass (CoM) per period, $\delta x = \bar{x}(T) - \bar{x}(0)$, during the adiabatic evolution after preparing a single-excitation initial state [13–15]. The CoM, expressed as

$$\bar{x} = \sum_j j\langle \hat{n}_j \rangle, \tag{10}$$

with $\hat{n}_j \equiv \hat{a}_j^\dagger \hat{a}_j$, can be extracted from the adiabatic evolution of the initial single-excitation state on the superconducting processor.

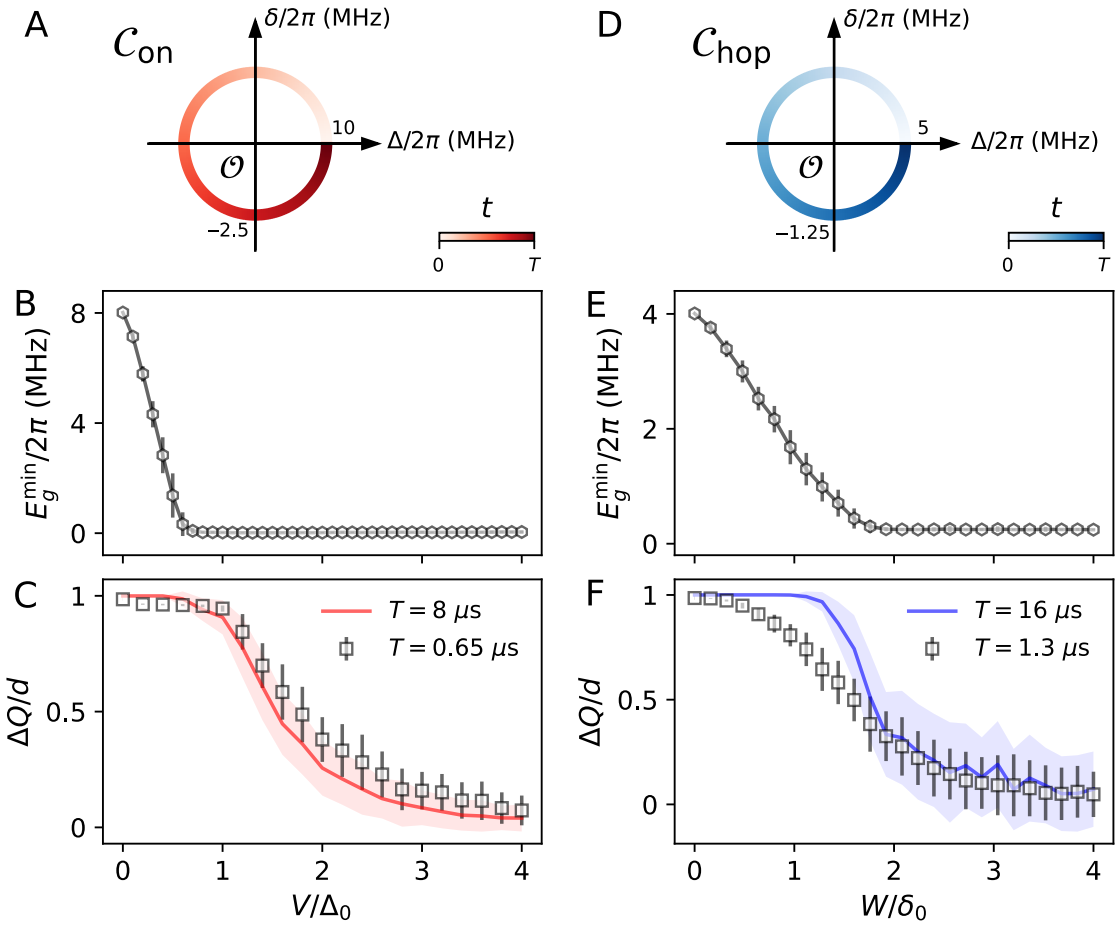

Supplementary Fig. 3. Bandgaps and transport in the Rice-Mele model with disorder. (**A**) Pumping trajectory $\mathcal{C}_{\rm on}$. (**B**) Minimum instantaneous gap, $E_g^{\rm min}$, versus the on-site random disorder strength V for the trajectory $\mathcal{C}_{\rm on}$. (**C**) Pumped amount, ΔQ, as a function of V for the trajectory $\mathcal{C}_{\rm on}$. (**D**) Pumping trajectory $\mathcal{C}_{\rm hop}$. (**E**) Minimum instantaneous gap, $E_g^{\rm min}$, versus the hopping random disorder strength W for the trajectory $\mathcal{C}_{\rm hop}$. (**F**) Pumped amount, ΔQ, as a function of W for the trajectory $\mathcal{C}_{\rm hop}$. All numerical simulations are averaged over 100 different disorder configurations, and the shaded regions and the error bars show the one standard deviation (1SD).

C. Pumping under disorder

In addition to the topological nature of Thouless pumping, we investigate the effects of on-site random disorder V_j on the topological pumping by substituting Δ in Supplementary Eq. (1) to $\Delta + V_j$, where V_j is uniformly distributed in the range $[-V, V]$. For an integrable 1D quantum system, an arbitrarily small amount of on-site disorder leads to localization [16]. However, robustness against weak disorder in topological quantum phenomena is expected [17]. Here, we numerically study the topology-disorder transition, in our superconducting processor.

We now consider the trajectory $\mathcal{C}_{\rm on}$ (Supplementary Fig. 3A),

$$(\Delta, \delta) = (\Delta_0 \cos(2\pi t/T), \delta_0 \sin(2\pi t/T)), \tag{11}$$

with $\Delta_0/2\pi$ =10.0 MHz, $\delta_0/2\pi$ =2.5 MHz, $J/2\pi$ =2.0 MHz, and $T = 0.65$ μs. We calculate the average of ΔQ for different values of V, for $T = 0.65$ μs and 8.0 μs. As shown in Sup-

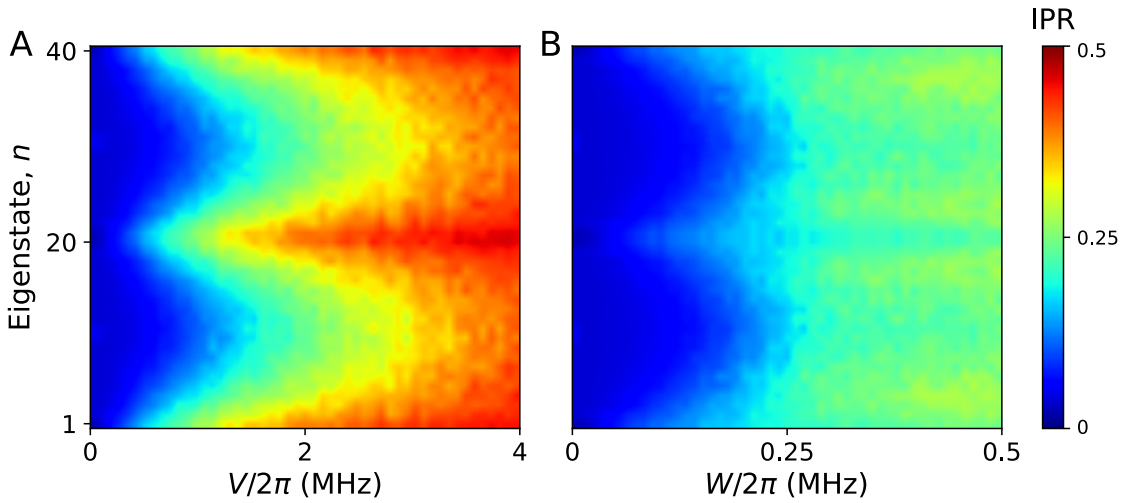

Supplementary Fig. 4. The inverse participation ratio (IPR) numerically calculated for the RM model with on-site and hopping disorder. (**A**) IPR of the n-th eigenstate against the on-site random disorder strength V for the trajectory $\mathcal{C}_{\rm on}$ at the SSH parameter point $(\Delta/2\pi, \delta/2\pi) = (0\,\mathrm{MHz}, 2.5\,\mathrm{MHz})$. (**B**) IPR of the n-th eigenstate against the hopping random strength W for the trajectory $\mathcal{C}_{\rm hop}$ at the parameter point $(\Delta/2\pi, \delta/2\pi) = (5\,\mathrm{MHz}, 0\,\mathrm{MHz})$. Both results are averaged with 100 different configurations of disorder.

plementary Fig. 3C, they both satisfy the adiabatic limit. Moreover, the crossover between the topological phase and the localized phase is related to the minimal many-body instantaneous gap [4, 7] (Supplementary Fig. 3B)

$$E_g^{\rm min} = \min_{\phi}[E_{N+1}(t) - E_N(t)], \tag{12}$$

where $E_N(t)$ is the N-particle ground state energy at time t. We observe that topological pumping persists with $\Delta Q/d = 1$, even with weak disorder $V/\Delta_0 \approx 1$, when the energy gap remains open to allow for a possible adiabatic evolution of the ground state, and $\Delta Q/d \approx 0$ with strong disorder satisfying $V/\Delta_0 \gtrsim 3$.

Moreover, we study the effect of hopping random disorder by substituting δ by $\delta + W_j$ in Supplementary Eq. (1) by taking W_j being uniformly distributed in the range $[-W, W]$. The trajectory $\mathcal{C}_{\rm hop}$ is chosen as an equally scaled-down version of $\mathcal{C}_{\rm on}$, with $\Delta_0/2\pi = 5.0$ MHz, $\delta_0/2\pi = 1.25$ MHz, $J/2\pi = 1.0$ MHz, and $T = 1.3$ μs, see Supplementary Fig. 3D. We observe in Supplementary Fig. 3F a decreasing behavior of ΔQ as the hopping disorder strength increases, which is similar to the case with on-site random disorder. Note that the non-adiabatic effect shows that the transition point moves toward a weaker disorder strength, by comparing the cases with periods $T = 1.3$ μs and 16 μs.

D. Localization in the Rice-Mele model with disorder

According to Anderson localization (AL), an integrable 1D system tends to be at a localized state with relatively strong on-site disorder. To characterize the localization phenomena of the RM model with disorder, we employ the real-space inverse participation ratio (IPR), which is defined

as

$$\mathcal{I}(|\psi_n\rangle) = \sum_j |\langle 1_j|\psi_n\rangle|^4, \tag{13}$$

where $|\psi_n\rangle$ is the n-th eigenstate, and $|1_j\rangle = \hat{a}_j^\dagger|0\rangle$ denotes a particle state with an excitation at site j. A large IPR signifies a strong localization tendency, and $\mathcal{I} \sim 1/L$ for a plane-wave state, while $\mathcal{I} = 1$ identifies a perfect localized state at the single site.

We calculate the IPR of the system with on-site random disorder at the so-called SSH parameter point, i.e., $(\Delta/2\pi, \delta/2\pi) = (0\,\mathrm{MHz}, 2.5\,\mathrm{MHz})$ of the trajectory $\mathcal{C}_{\mathrm{on}}$. Fig. 4A clearly shows that the system tends to be at a localized state as the disorder strength becomes large. Note that the transition point between the topological phase and the localized phase, $V_{\mathrm{c}} \simeq 0.2$ MHz, is much smaller than the trajectory radius $\Delta_0/2\pi = 10$ MHz. Although the instantaneous Hamiltonian eigenstates are shown in Supplementary Fig. 4A to be localized with a small on-site disorder strength, the topological transport remains robust against weak disorder. It was shown [7] that the breakdown of pumping under on-site disorder is linked to the delocalization-localization transition of the single-particle Floquet eigenstates instead of instantaneous eigenstates.

Similar to the case with on-site random disorder, an integrable 1D system tends to be localized under considerable hopping random disorder, but with a distinct law [18–20]. When only hopping random disorder is involved, the localization length of the zero-energy state is infinite. Nevertheless, the state should be considered to be localized due to the fact that the mean values of the transmission coefficient approach zero in the thermodynamic limit.

In analogy to the SSH parameter point, we compute the IPR for the trajectory $\mathcal{C}_{\mathrm{hop}}$ with hopping disorder at the parameter point $(\Delta/2\pi, \delta/2\pi) = (5\,\mathrm{MHz}, 0\,\mathrm{MHz})$, see Supplementary Fig. 4B. The numerical results show that the IPR increases as the disorder strength increases, suggesting that instantaneous eigenstates tend to be localized with relatively strong disorder. Similarly, the transition point of instantaneous eigenstates is much smaller than the breakdown point of pumping. Therefore, it is still unclear whether the behavior of ΔQ could characterize the delocalization-localization transition of the single-particle Floquet eigenstates, which deserves further investigations.

E. Double-loop pumping induced by on-site disorder

Connecting two elliptical loops with opposite directions, the double-loop trajectory, $\mathcal{C}_{\mathrm{dl}}$, as shown in Supplementary Fig. 5A, is topologically trivial in the clean limit; because of the addition of two inverse Chern numbers [8, 21]. Topological pumping would be realizable, if disorder asymmetrically inhibits the topology of the two pumping loops.

Here, we now study a double-loop trajectory consisting of one two half outer loops $\mathcal{C}_{\mathrm{on}}$ and one complete inter loop $\mathcal{C}_{\mathrm{on1}}$ in an inverse direction, as shown in Supplementary Fig. 5**A**, which is expected to exhibit similar topological transport behaviors with on-site random disorder, similar as the case discussed in Ref. [21].

The trajectory, $\mathcal{C}_{\mathrm{dl}}$, can be parameterized as $(\Delta(t), \delta(t))$ with

$$\Delta(t) = \begin{cases} \Delta_0 \cos\Omega_1 t, & \text{for } 0 < t \le 3\tau_1/4, \\ -\Delta_1 \sin\Omega_2(t - 3\tau_1/4), & \text{for } 3\tau_1/4 < t \le 3\tau_1/4 + \tau_2, \\ \Delta_0 \sin\Omega_1(t - 3\tau_1/4 - \tau_2), & \text{for } 3\tau_1/4 + \tau_2 < t \le \tau_1 + \tau_2, \end{cases} \tag{14}$$

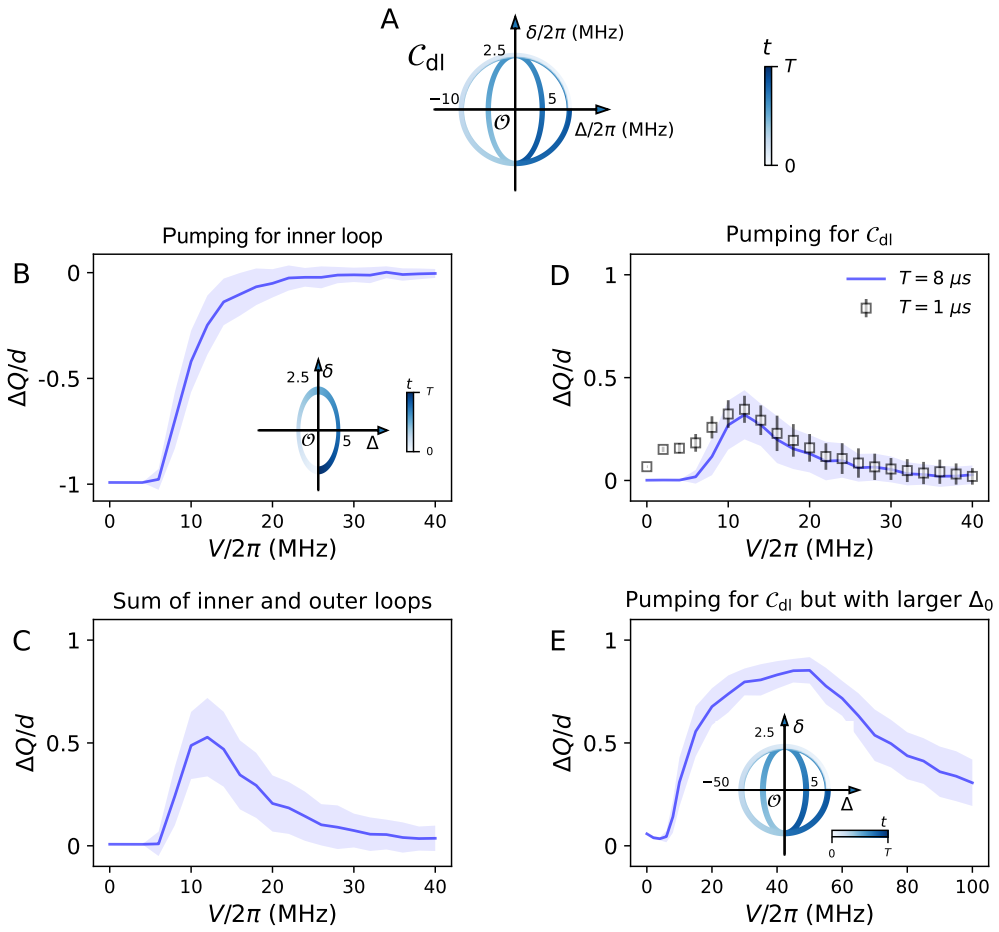

Supplementary Fig. 5. Topological pumping with on-site random disorder for the double-loop trajectory, $\mathcal{C}_{\rm dl}$. (**A**) Trajectory $\mathcal{C}_{\rm dl}$, containing an incomplete counterclockwise outer loop, and a complete clockwise inner loop. (**B**) Pumped amount, ΔQ, versus the disorder strength V for the inner loop. (**C**) ΔQ versus V for the complete outer loop, corresponding to the result in Supplementary Fig. 3**C**, and ΔQ versus V for the inner loop. (**D**) ΔQ versus V for $\mathcal{C}_{\rm dl}$ with $T = 1$ μs and 8 μs, respectively. (**E**) Quantized topological pumping induced by on-site random disorder with sufficiently separated Δ_0 and Δ_1, where $\Delta_0/2\pi = 50$ MHz, and $\Delta_1/2\pi = 5$ MHz.

$$\delta(t) = \begin{cases} \delta_0 \sin \Omega_1 t, & \text{for } 0 < t \le 3\tau_1/4, \\ -\delta_0 \cos \Omega_2 (t - 3\tau_1/4), & \text{for } 3\tau_1/4 < t \le 3\tau_1/4 + \tau_2, \\ -\delta_0 \cos \Omega_1 (t - 3\tau_1/4 - \tau_2), & \text{for } 3\tau_1/4 + \tau_2 < t \le \tau_1 + \tau_2, \end{cases} \tag{15}$$

with $\Delta_0/2\pi = 10$ MHz, $\Delta_1/2\pi = 5$ MHz, $\delta_0/2\pi = 2.5$ MHz, $J/2\pi = 2$ MHz, $\Omega_1 = 2\pi/\tau_1$, $\Omega_2 = 2\pi/\tau_2$, and $T = 2\tau_1 = 2\tau_2 = 1$ μs. We show ΔQ of $\mathcal{C}_{\rm on1}$ versus the on-site disorder strength in Supplementary Fig. 5B and a summation of ΔQ for $\mathcal{C}_{\rm on}$ and $\mathcal{C}_{\rm on1}$ in Supplementary Fig. 5C. These numerical results demonstrate topological pumping induced by moderate on-site disorder. In addition, we directly calculate ΔQ of $\mathcal{C}_{\rm dl}$ versus the disorder strength, which matches well with the summation of ΔQ for two loops, see Supplementary Fig. 5D.

Quantized topological pumping occurs when Δ_0 and Δ_1 are sufficiently far apart, such that an

appropriate disorder strength V is strong enough for the inner loop $\mathcal{C}_{\rm on1}$, but still too weak for the outer loop $\mathcal{C}_{\rm on}$. We numerically simulate another trajectory with identical parameters to $\mathcal{C}_{\rm dl}$ except for $\Delta_0/2\pi = 50$ MHz, where a quantized plateau is observed, see Supplementary Fig. 5E.

F. Single-loop pumping induced by hopping disorder

In the clean limit, the trajectory with a circle outside the origin centered on the δ-axis, $\mathcal{C}_{\rm sl}$, as shown in Supplementary Fig. 6A, leads to a topologically trivial pumping phenomenon with a winding number of 0. By introducing an appropriate hopping random disorder strength, a nonzero ΔQ occurs, because the gapless point (line) possibly moves inside the trajectory. However, pumping is not quantized, precluding the adiabatic limit, due to the rapid closure of the band gap. Fortunately, an intrinsic topologically nontrivial quantized pumping scheme, induced by quasi-periodic intracell hopping disorder with gap reopening, has been proposed in Ref. [8].

Given the parameterized path, $\mathcal{C}_{\rm sl}$, parameterized with $(\Delta, \delta) = (\Delta_0 \cos\phi, \delta_c + \delta_0 \sin\phi)$, with $\Delta_0/2\pi = 5$ MHz, $\delta_0/2\pi = 1.0$ MHz, $\delta_c/2\pi = 1.2$ MHz, and $J/2\pi = 1.8$ MHz, we calculate $E_g^{\rm min}$ and ΔQ against random hopping disorder $W_j \in [-W, W]$, and quasi-periodic intracell hopping disorder

$$W'_{j=2k} = W_p \cos(2\pi\alpha k + \beta), \tag{16}$$

where $\alpha = (\sqrt{5}-1)/2$ is an irrational number. Although ΔQ becomes nonzero with an intermediate random disorder strength $W/2\pi \gtrsim 2$ MHz, the minimum gap closes, resulting in a non-quantized pumping with large sample-to-sample fluctuations, see Figs. 6B and 6C. In comparison, the gap can reopen with quasi-periodic hopping disorder, and one quantized plateau is observed at 1.5 MHz $\lesssim W_p/2\pi \lesssim 3$ MHz, see Supplementary Fig. 6D and 6E. The spectra under different quasiperiodic disorder is shown in Supplementary Fig. 8, which can be also observed by dynamical spectrum technique [1]. The increase of ΔQ with a short period $T = 1.4$ μs provides an opportunity for an experimental demonstration of Thouless pumping induced by quasi-periodic disorder, as a dynamical analog of topological Anderson insulator (TAI) in Ref. [8]. To exactly obtain the range of disorder, where the plateau appears, we plot ΔQ for different disorder strengths and periods, see Supplementary Fig. 7. The numerical results indicate that the quantized plateau can be observed, when 1.6 MHz $\leq W_p/2\pi \leq 2.9$ MHz, in the adiabatic limit. Although the maximum of ΔQ decreases with the descent of period, the peak between the parameter region indicated by the Chern number, i.e., the dashed line in Supplementary Fig. 7, retains.

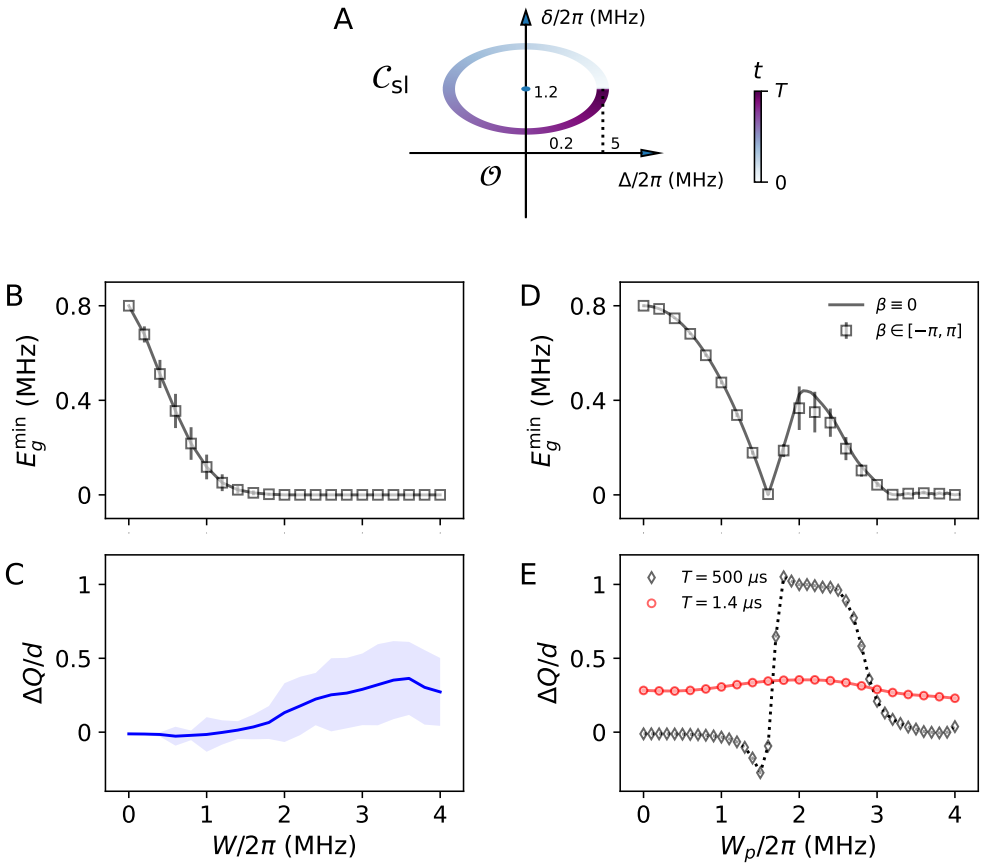

Supplementary Fig. 6. Topological pumping with hopping random disorder and quasi-periodic intracell hopping disorder for the single-loop trajectory, $\mathcal{C}_{\rm sl}$. (**A**) The single-loop trajectory $\mathcal{C}_{\rm sl}$, containing a circle centered at the point $(0, \delta_c)$ on the δ-axis and being outside of the origin in the Δ-δ plane. (**B**) The minimum instantaneous gap, $E_g^{\rm min}$, versus hopping random disorder strengths W. (**C**) The pumped amount, ΔQ, against W for $T = 500$ μs. The calculation result of ΔQ is averaged over 100 different disorder samples, and the shaded regions and the error bars show the range of one standard deviation. (**D**) $E_g^{\rm min}$ versus the quasi-periodic intracell hopping disorder strength W_p with the phase β fixed at 0 and taken from the uniform distribution in the range $[-\pi, \pi]$, respectively. (**E**) ΔQ against W_p for $T = 1.4$ μs and 500 μs, showing a quantized plateau. The lattice size is $L = 800$ for the numerical calculation of the band gap.

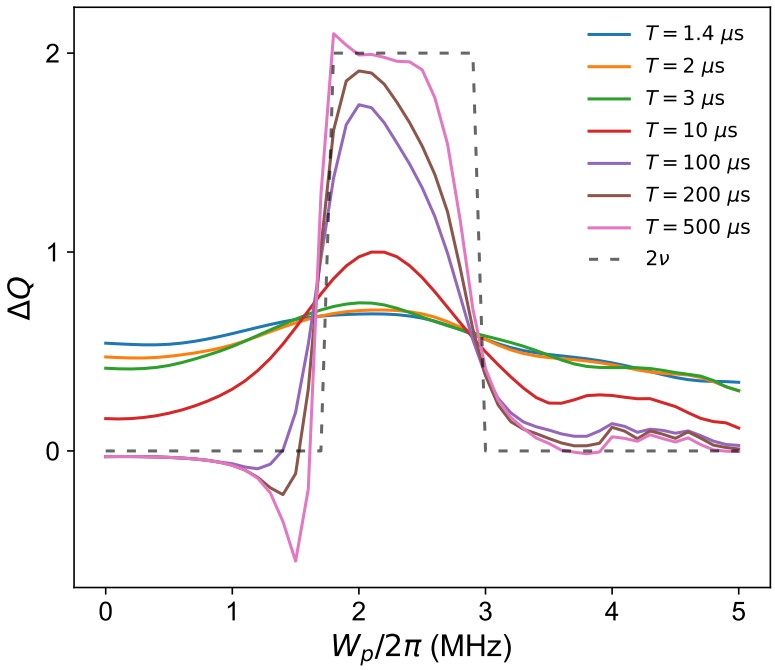

Supplementary Fig. 7. Pumping for the trajectory, $\mathcal{C}_{\rm sl}$, with quasi-periodic intracell hopping disorder for different periods. The dashed line in the Chern number obtained by numerical results. The quantized plateau appears when the disorder strength, $W_p/2\pi$, varies between around 1.6 MHz and 2.9 MHz, indicated by two dashed-dotted lines.

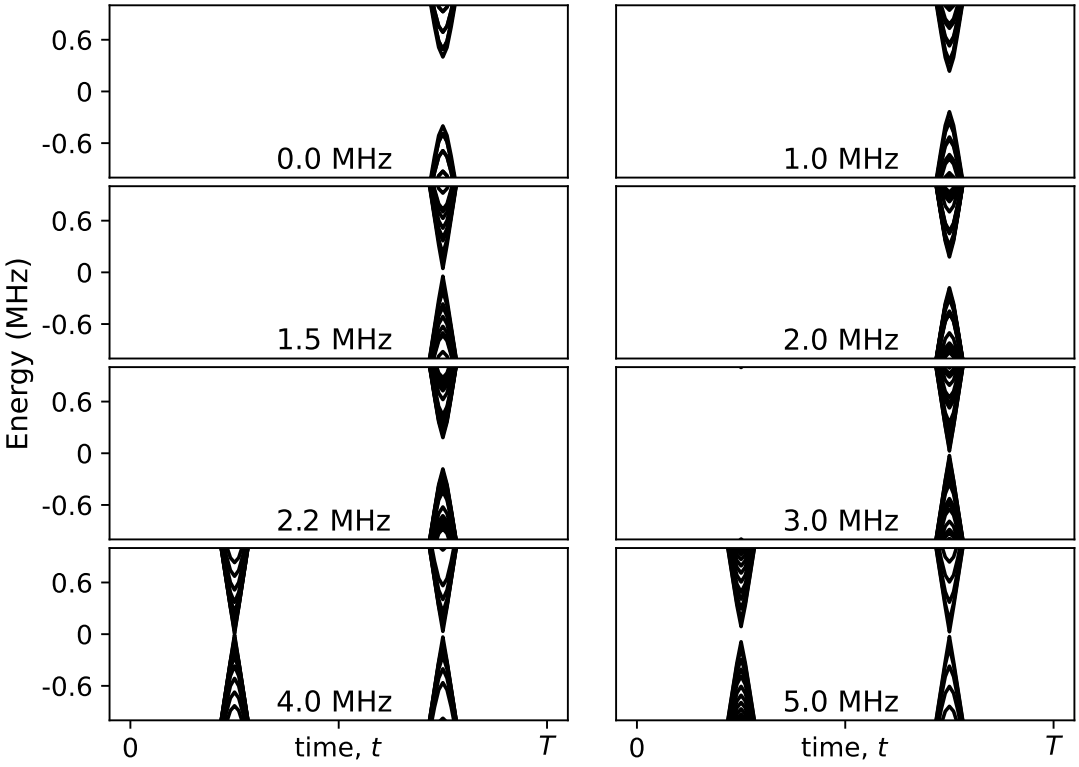

Supplementary Fig. 8. Instantaneous energy spectra of the bulk under quasi-periodic disorder. The results are averaged over 100 disorder realizations.

Supplementary Note III: Floquet Engineering for Adiabatic Systems

Floquet engineering has been applied in superconducting quantum circuits as an effective method to modulate the hopping strength of a time-independent quantum many-body system [1, 22]. In our 1D 41-qubit superconducting processor, the effective Hamiltonian of two nearest-neighboring qubits can be described as

$$\hat{H} = -\omega_j(t)\hat{\sigma}_j^z/2 - \omega_{j+1}(t)\hat{\sigma}_{j+1}^z/2 + g_{j,j+1}(\hat{\sigma}_j^+\hat{\sigma}_{j+1}^- + \text{H.c.}), \tag{17}$$

where $\omega_j(t)$ denotes the j-th qubit frequency, $\hat{\sigma}_j^{x,y,z}$ are Pauli matrices with $\hat{\sigma}_j^{\pm} = (\hat{\sigma}_j^x \pm \mathrm{i}\hat{\sigma}_j^y)/2$, $g_{j,j+1}$ is the coupling strength between the j-th and $(j+1)$-th qubits. With the method introduced in Ref. [1], the effective hopping strength can be modulated as

$$g_{j,j+1}^{\text{eff}} = g_{j,j+1} J_0\left(\frac{\eta_j A_j - \eta_{j+1} A_{j+1}}{\mu}\right), \tag{18}$$

when we apply a microwave to manipulate the qubit frequency as

$$\omega_j(t) = \bar{\omega} + A_j \sin(\mu t + \varphi_0), \tag{19}$$

where A_j and μ denote the modulation amplitude and the frequency, respectively, $\bar{\omega}$ is the average qubit frequency, φ_0 is a common initial phase, $J_s(x)$ is the s-order Bessel function, and $\eta_j \approx 1$ is the scale factor corresponding to the experimental calibration.

A. Adiabatic condition

In the Rice-Mele model Hamiltonian (1), the simultaneous adiabatic changes of the on-site and hopping terms result in a two-qubit Hamiltonian:

$$\hat{H}' = \Delta_j(t)\hat{n}_j + \Delta_{j+1}(t)\hat{n}_{j+1} + \delta_{j,j+1}(t)(\hat{a}_j^\dagger \hat{a}_{j+1} + \hat{a}_j \hat{a}_{j+1}^\dagger). \tag{20}$$

Then the Hamiltonian in the interaction picture can be expressed as

$$\hat{H}_I' = \delta_{j,j+1}(t) \exp\left\{\mathrm{i}\int_0^t \mathrm{d}t\ \Delta(t)\right\} \hat{a}_j^\dagger \hat{a}_{j+1} + \text{H.c.}, \tag{21}$$

where $\Delta(t) \equiv \Delta_j(t) - \Delta_{j+1}(t)$. Intuitively, if $\delta_j(t)$ and $\Delta_j(t)$ vary slowly enough, we could generalize Supplementary Eq. (19) to

$$\omega_j(t) = \bar{\omega} + \Delta_j(t) + A_j(t)\sin(\mu t + \varphi_0), \tag{22}$$

where

$$A_j(t) = \frac{1}{\eta_j}\left[\eta_{j+1}A_{j+1}(t) \mp \mu J_0^{-1}\left(\frac{\delta_{j,j+1}(t)}{g_{j,j+1}}\right)\right]. \tag{23}$$

More specifically, if we denote the cut-off frequency of $\delta_j(t)$ and $\Delta_j(t)$ as δ_j^c and Δ_j^c, the adiabatic condition will be expressed as

$$\delta_j^c, \Delta_j^c \ll \mu. \tag{24}$$

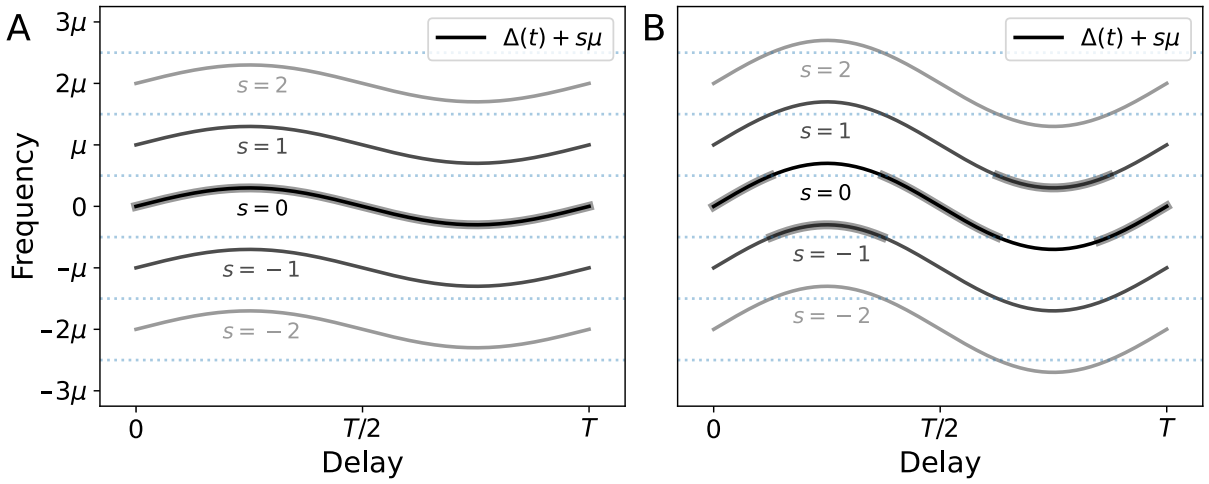

Supplementary Fig. 9. Bands of frequencies inside **(A)** and outside **(B)** the Nyquist condition. The thick solid lines represent the effective band under the rotating wave approximation (RWA). The lowest-order term remains $\Delta(t)$, when $\mu > 2\max_t |\Delta(t)|$ is satisfied; otherwise, the effective band consists of parts of the bands $s = \pm 1$.

B. Nyquist condition

When the qubit frequency is adjusted to be as in Supplementary Eq. (22), the unitary transformation in the interaction picture is written as

$$\hat{U}_I(t) \approx \prod_{n=j,j+1} \exp\left\{ \mathrm{i}\left(\bar{\omega} t + \int_0^t \mathrm{d}t \, \left[\Delta_n(t) - \frac{A_n(t)}{\mu} \cos(\mu t + \varphi_0) \right] \right) \hat{n}_j \right\}, \tag{25}$$

and the effective Hamiltonian can be obtained as

$$\begin{aligned}
\hat{H}_I' =& \hat{U}_I(t)\hat{H}(t)\hat{U}_I^\dagger(t) + \mathrm{i}\left[\frac{\mathrm{d}}{\mathrm{d}t}\hat{U}_I(t)\right]\hat{U}_I^\dagger(t), \\
=& g_{j,j+1} \exp\left\{ \mathrm{i}\int_0^t \mathrm{d}t \, \Delta(t) \right\} \exp\left\{ \mathrm{i}\frac{A_j(t)}{\mu}\cos(\mu t + \varphi_0) \right\} \exp\left\{ -\mathrm{i}\frac{A_{j+1}(t)}{\mu}\cos(\mu t + \varphi_0) \right\} \hat{a}_j^+ \hat{a}_{j+1} + \mathrm{H.c.} \\
=& g_{j,j+1} \exp\left\{ \mathrm{i}\int_0^t \mathrm{d}t \, \Delta(t) \right\} \sum_{m,n=-\infty}^{+\infty} \mathrm{i}^{m+n} J_m\left(\frac{A_j(t)}{\mu}\right) J_n\left(-\frac{A_{j+1}(t)}{\mu}\right) \mathrm{e}^{\mathrm{i}(m+n)(\mu t+\varphi_0)} \hat{a}_j^+ \hat{a}_{j+1} + \mathrm{H.c.} \\
=& g_{j,j+1} \exp\left\{ \mathrm{i}\int_0^t \mathrm{d}t \, \Delta(t) \right\} \sum_{s=-\infty}^{+\infty} \sum_{m+n=s} \mathrm{i}^{m+n} J_m\left(\frac{A_j(t)}{\mu}\right) J_n\left(-\frac{A_{j+1}(t)}{\mu}\right) \mathrm{e}^{\mathrm{i}(m+n)(\mu t+\varphi_0)} \hat{a}_j^+ \hat{a}_{j+1} + \mathrm{H.c.} \\
=& g_{j,j+1} \exp\left\{ \mathrm{i}\int_0^t \mathrm{d}t \, \Delta(t) \right\} \sum_{s=-\infty}^{+\infty} \exp\left\{ \mathrm{i}s(\mu t + \frac{\pi}{2} + \varphi_0) \right\} J_s\left(\frac{A_{j+1}(t) - A_j(t)}{\mu}\right) \hat{a}_j^+ \hat{a}_{j+1} + \mathrm{H.c.}.
\end{aligned} \tag{26}$$

Compared with Eq. (21), Supplementary Eq. (26) indicates that the Hamiltonian is composed of bands of frequencies, i.e., $\Delta(t) + s\mu$. According to the rotating wave approximation (RWA), high-frequency oscillatory terms are neglected, and low-frequency terms contribute predominantly. The

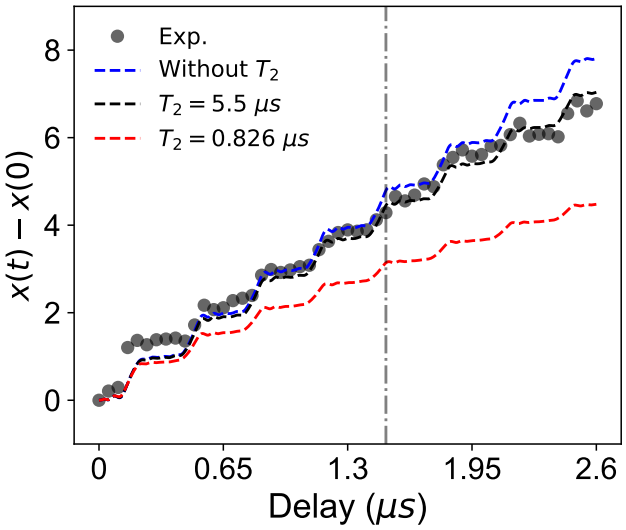

Supplementary Fig. 10. Experimental and numerical time evolution for topological pumping with different dephasing time T_2. The dark dots are experimental data, the blue, black and red curves are numerical simulations without dephasing, with $T_2 = 5.5$ μs and $T_2 = 0.826$ μs, respectively.

necessary and sufficient condition for frequency band components to have no overlap with each other in the frequency domain is

$$\mu > 2 \max_t |\Delta(t)|, \tag{27}$$

as shown in Figs. 9A and 9B. Inequality (27) is called the Nyquist condition, named after the Nyquist's sampling theorem [23]. When both Supplementary Eq. (24) and Supplementary Eq. (27) are satisfied, Supplementary Eq. (26) approximates to Supplementary Eq. (21).

Supplementary Note IV: Additional Experimental Data

A. Effects of decoherence

The effects of decoherence, due to the interactions with the environment, are unavoidable in practical quantum simulations. In general, the influence on qubits can be classified into the energy relaxation effect, characterized by T_1, and the dephasing effect, identified by T_φ. As previously reported [24, 25], the effective dephasing time of a system with interactions is longer than the individually calibrated dephasing time T_2^*, due to the fact that eigenenergies of interacting systems depend weakly on each qubit flux.

Numerically, we calculate the topological pumping for the trajectory $\mathcal{C}_4$ introduced in the main text, with consideration of dephasing for a 12-qubit chain, using the Lindblad master equation. For simplicity, we assume that all qubits have a uniform dephasing time to estimate the effective T_2 quantitatively. The direct comparison of numerical and experimental results is shown in Supplementary Figure 10. We find that there is a good match between the experimental time evolution and the one obtained by numerical calculation when T_2 is chosen as 5.5 μs. A deviation occurs when the evolution time beyond $3T$, due to the effect of short dephasing time. Moreover, we calibrated the states with a conserved particle number for the single-excitation or double-excitation initial states to mitigate the influence of energy relaxation. Overall, we conclude that our device

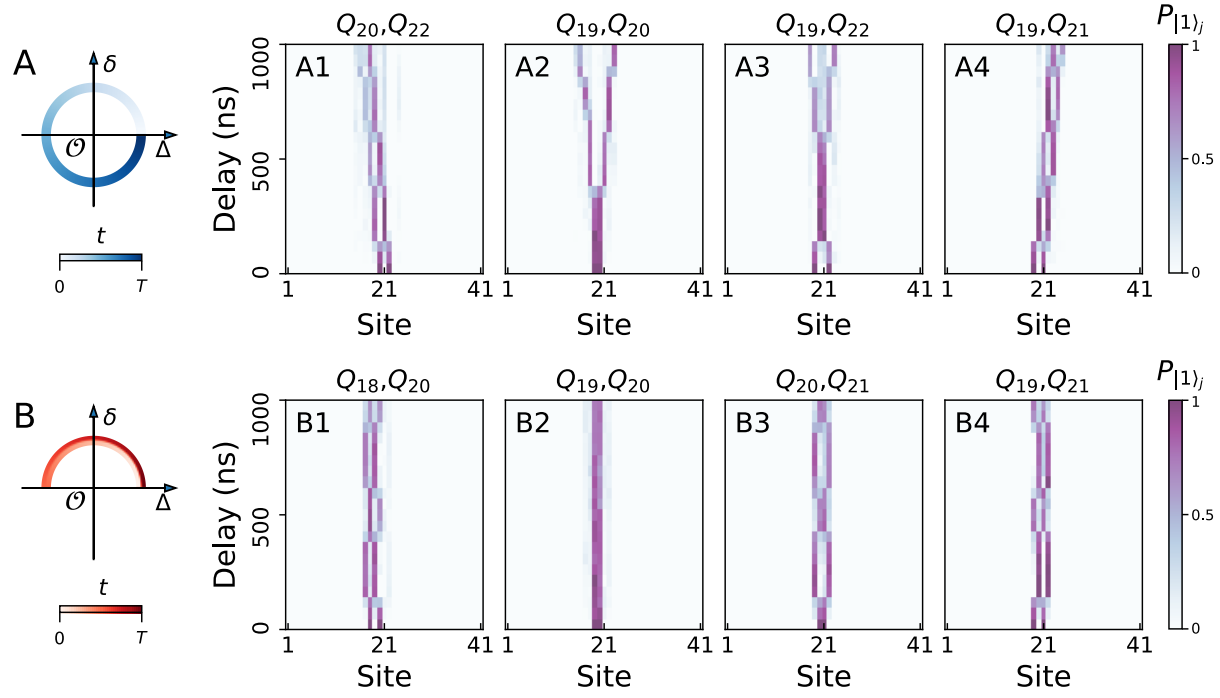

Supplementary Fig. 11. Thouless Pumping with two-photon excitation. (**A1**–**A4**) Experimental results of the time evolutions of the two-excitation states after initially exciting different qubits pairs for the trajectory in **A**. (**B1**–**B4**) Experimental results of the time evolutions of the two-excitation states by exciting different qubits pairs for the trajectory in **B**.

can be approximately regarded as a closed quantum system when the experimental time within 1500 ns.

B. Pumping of double excitations

We also perform double-excitation experiments in the clean limit for two different trajectories. The trajectory as shown in Supplementary Figure 11A is $(\Delta_0 \sin(2\pi t/T), \delta_0 \cos(2\pi t/T))$, with $\Delta_0/2\pi = 10$ MHz, $\delta_0/2\pi = 2.5$ MHz, and $T = 500$ ns, and the second trajectory as plotted in Supplementary Figure 11B is $(\Delta_0 \cos(2\pi t/T), \delta_0 |\sin(2\pi t/T)|)$ with the same parameters.

Since the initial excitations, prepared at odd and even sites, have opposite winding numbers in the RM model (1), ΔQ depends on both the trajectory and the parity combination of sites. In addition to the non-zero winding number, the condition that parity of the excited sites is the same, is required for topological nontrivial pumping. By exciting different qubits pairs, we obtain distant patterns of QWs as shown in Figs. 11A1–A4, and 11B1–B4. Experimental results reveal that pumping of two-photon behaves like the transportation of two single-photons without interaction due to the fact that our system satisfies the hard-core limit [26].

C. Pumping under on-site and hopping random disorder

The experimental results of the single-photon excitation probabilities for the trajectory $\mathcal{C}_{\rm on}$ versus the on-site random disorder V are plotted in Figs. 12. The displacement of the CoM per cycle,

δx, remains about two sites with weak disorder strength $0\,\mathrm{MHz} \leq V/2\pi \lesssim 8\,\mathrm{MHz}$. The displacement of the CoM per cycle, δx, decreases to about $0\,\mathrm{MHz}$ with a strong disorder strength $V/2\pi \gtrsim 28\,\mathrm{MHz}$. Intuitively, the propagation with a considerably strong disorder is almost localized at the initial site, due to localization.

The experimental results of the single-photon excitation probabilities for the trajectory $\mathcal{C}_{\mathrm{hop}}$ versus the hopping random disorder strength W are shown in Figs. 14. Similar to pumping with on-site random disorder, δx persists about 2 even with a weak disorder strength and drops with a relatively strong disorder strength, as discussed in the Supplementary Note II C. More specifically, $\delta x \approx 2$ when $0\,\mathrm{MHz} \leq W/2\pi \lesssim 0.8\,\mathrm{MHz}$, and $\delta x \approx 0$ when $W/2\pi \gtrsim 2.8\,\mathrm{MHz}$.

Therefore, *we experimentally observe a competition between topology and disorder in Thouless pumping. With both on-site and hopping disorder, the quantized charge transport* (or change of polarization), indicated by the Chern number, *is robust against disorder, for weak disorder, and breaks down when the disorder strength becomes relatively strong*.

D. Pumping induced by on-site random disorder

By engineering the RM model Hamiltonian parameterized with (Δ, δ) as shown in Eqs. (14) and (15), we can study pumping for the double-loop trajectory $\mathcal{C}_{\mathrm{dl}}$. First, we show δx versus the periods of two individual loop, τ_1 and τ_2, to determine the appropriate evolving time. The numerical results, as plotted in Supplementary Figure 13, indicate that δx is almost 0 when $\tau_1 = \tau_2 = 500$ ns, meaning the absence of topological pumping. Then, we show δx versus the on-site random disorder strength V. The results shown in Supplementary Figure 15 demonstrate topological transport occurs with a moderate disorder strength in the range $5\,\mathrm{MHz} \lesssim V/2\pi \lesssim 20\,\mathrm{MHz}$, indicating that topological pumping can be induced by on-site random disorder, and δx drops to zero again when the disorder strength increases up to $V/2\pi \gtrsim 25\,\mathrm{MHz}$.

E. Pumping induced by quasi-periodic hopping disorder

Quantized pumping is absent in the presence of random hopping disorder for the trajectory $\mathcal{C}_{\mathrm{sl}}$, as plotted in Supplementary Figure 6A. However, topological pumping may occur when applying quasi-periodic hopping disorder as discussed in Supplementary Note. II F. We show δx versus the quasi-periodic intracell hopping disorder strength W_p in Supplementary Figure 16. Although $\delta x \approx 0.4$ is still nonzero even in the clean limit due to the non-adiabatic effect, the rising of δx is captured as W_p increases. In addition, $\delta x > 0.9$ is observed when $1.2\,\mathrm{MHz} \lesssim W_p/2\pi \lesssim 2.7\,\mathrm{MHz}$, *implying the existence of Thouless pumping induced by quasi-periodic disorder*. In our experiments, the experimental scanning range of $W_p/2\pi$ is set up to 3 MHz due to the limitation of Floquet engineering in our device.

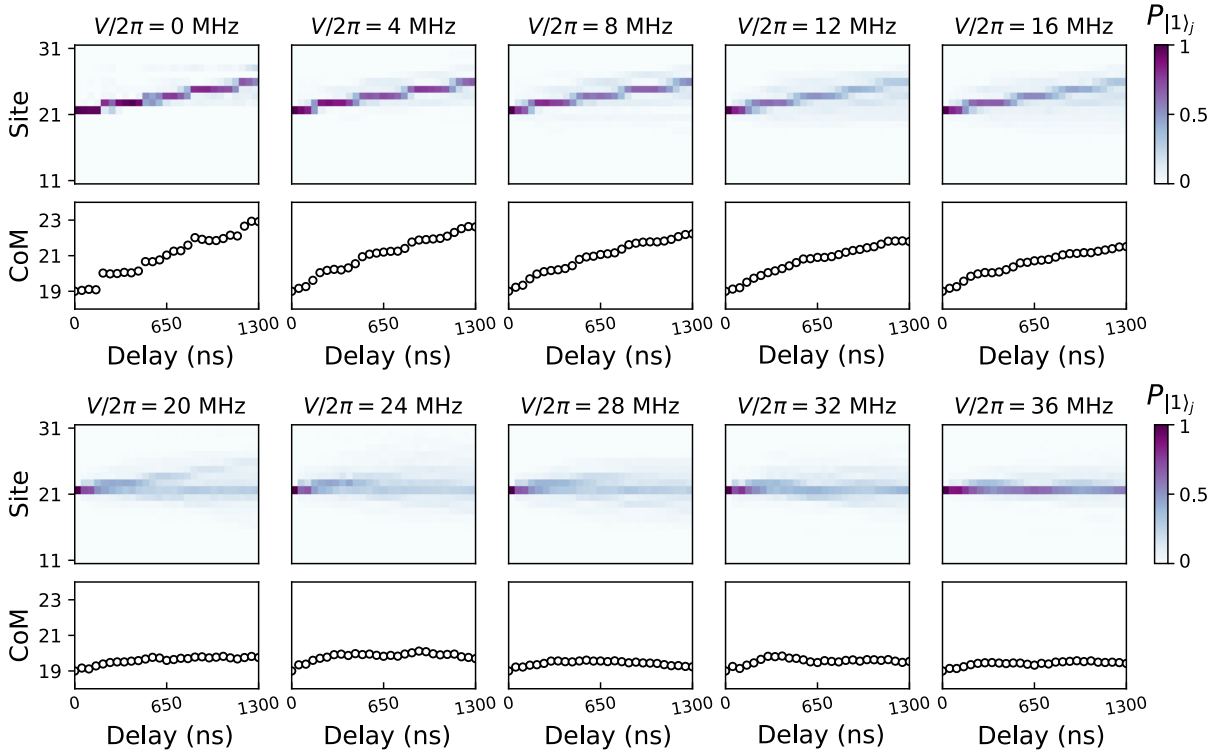

Supplementary Fig. 12. Experimental data of time evolutions of excitation probabilities and CoMs of pumping with on-site random disorder strengths ranging from $V/2\pi = 0$ MHz to 36 MHz. Topological pumping is robust against weak disorder strength and breaks down with a relatively strong disorder strength.

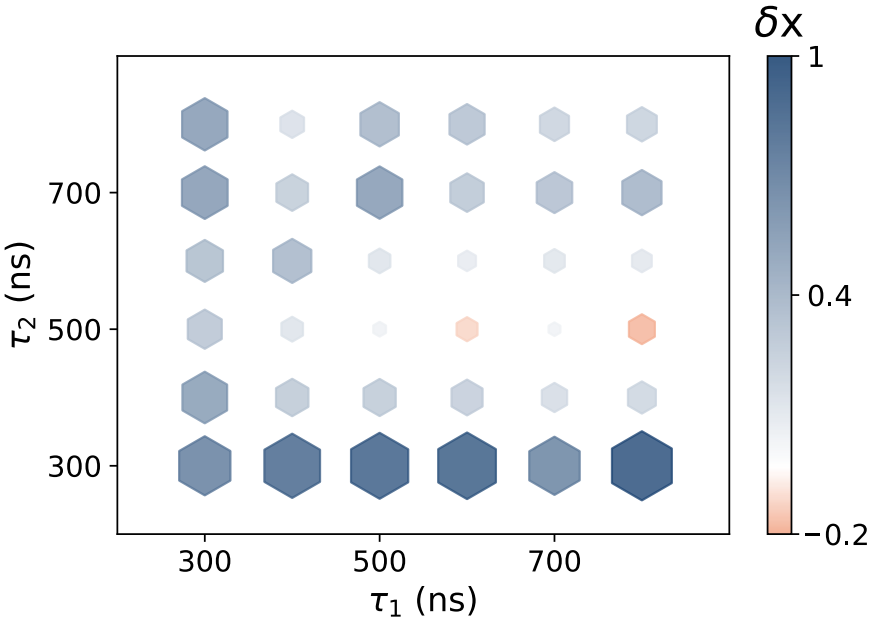

Supplementary Fig. 13. Experimental data of the displacement of CoM per cycle, δx for pumping via the double-loop trajectory $\mathcal{C}_{\rm dl}$ against different periods τ_1 and τ_2. The results indicate that no quantized transport of two opposite-direction loops occurs with equal periods of two loops $\tau_1 = \tau_2 = 500$ ns.

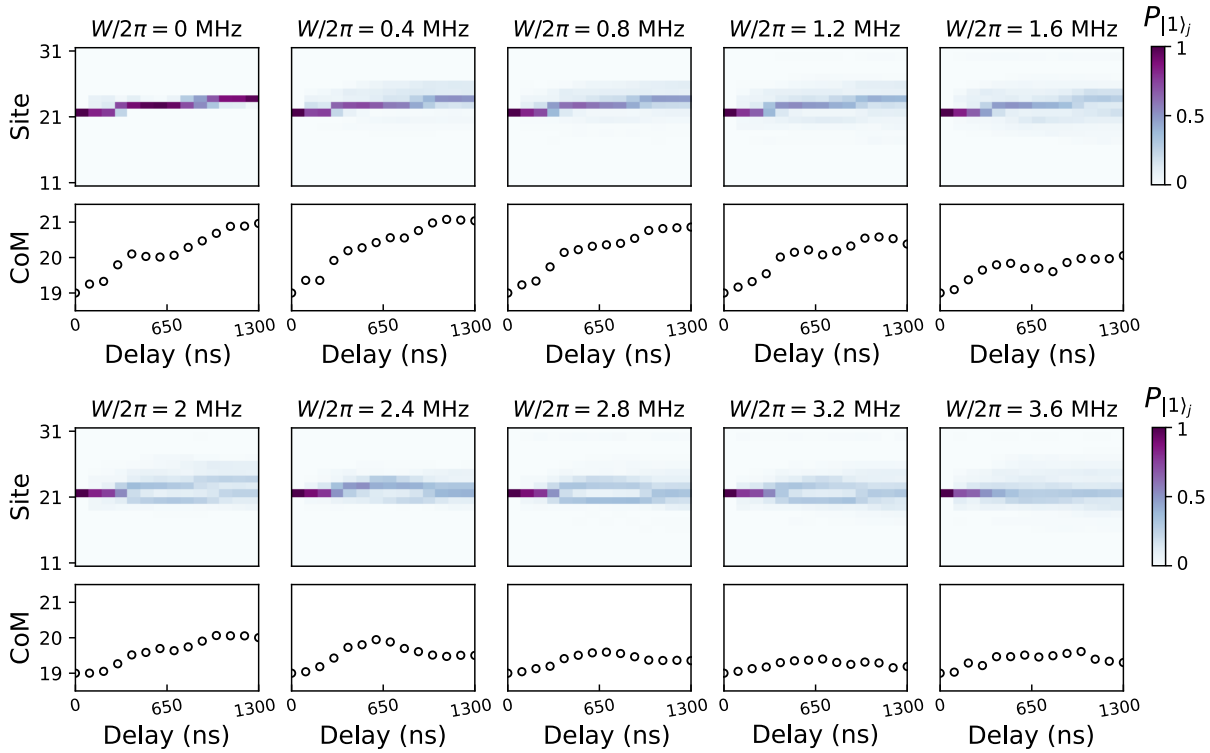

Supplementary Fig. 14. Experimental data of time evolutions of excitation probabilities and CoMs of pumping versus the hopping disorder strength ranging from $W/2\pi = 0$ MHz to 3.6 MHz. Similar as pumping with on-site random disorder, the quantized transport is robust against weak disorder and breaks down with strong disorder.

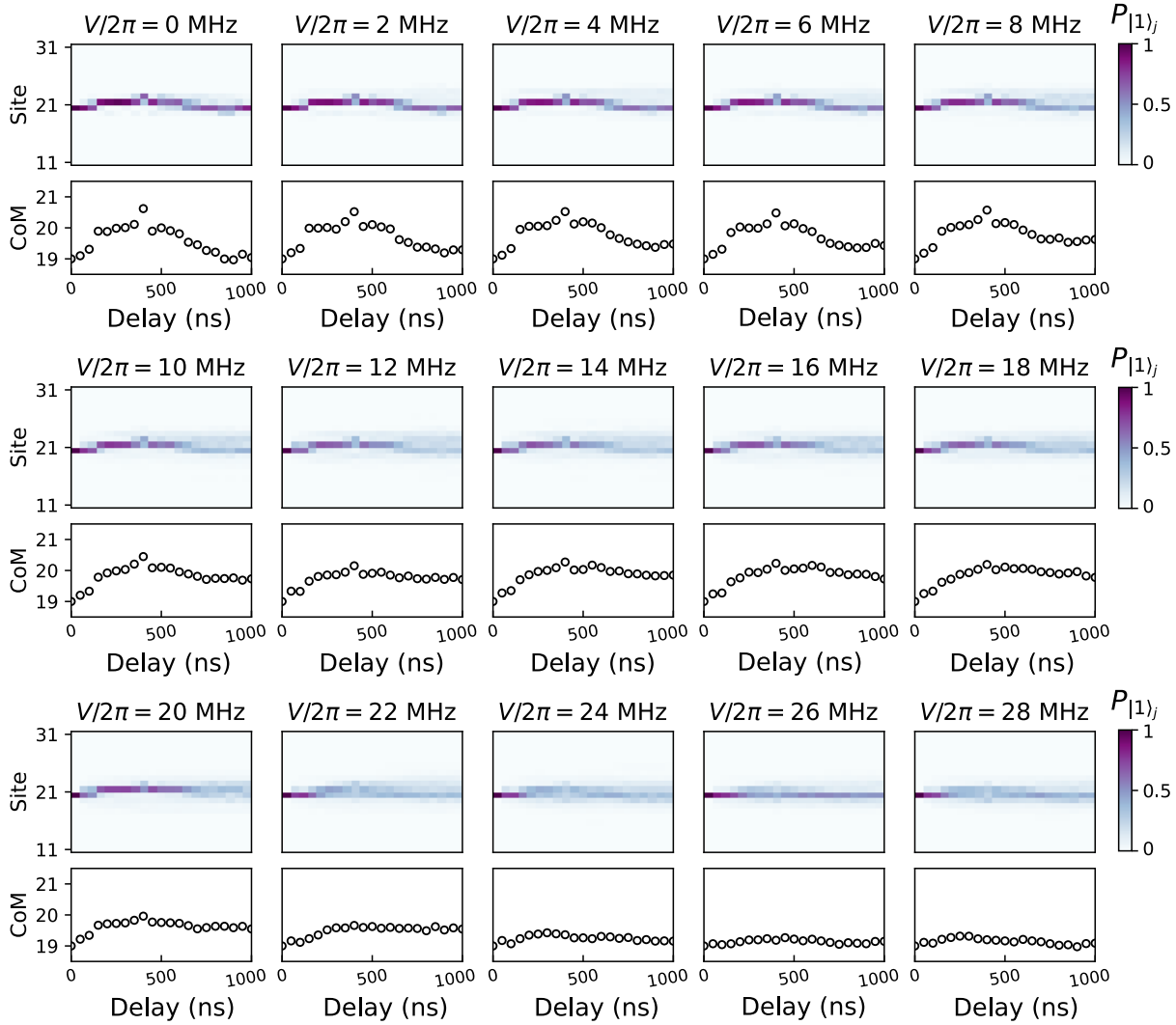

Supplementary Fig. 15. Experimental data of time evolutions of excitation probabilities and CoMs of pumping for the double-loop trajectory $\mathcal{C}_{\mathrm{dl}}$ versus the on-site random disorder strength V. The pumped amount ΔQ approximates 0 in the clean limit, but *quantum transport is observed with a moderate disorder strength and disappears again when disorder is strong enough.*

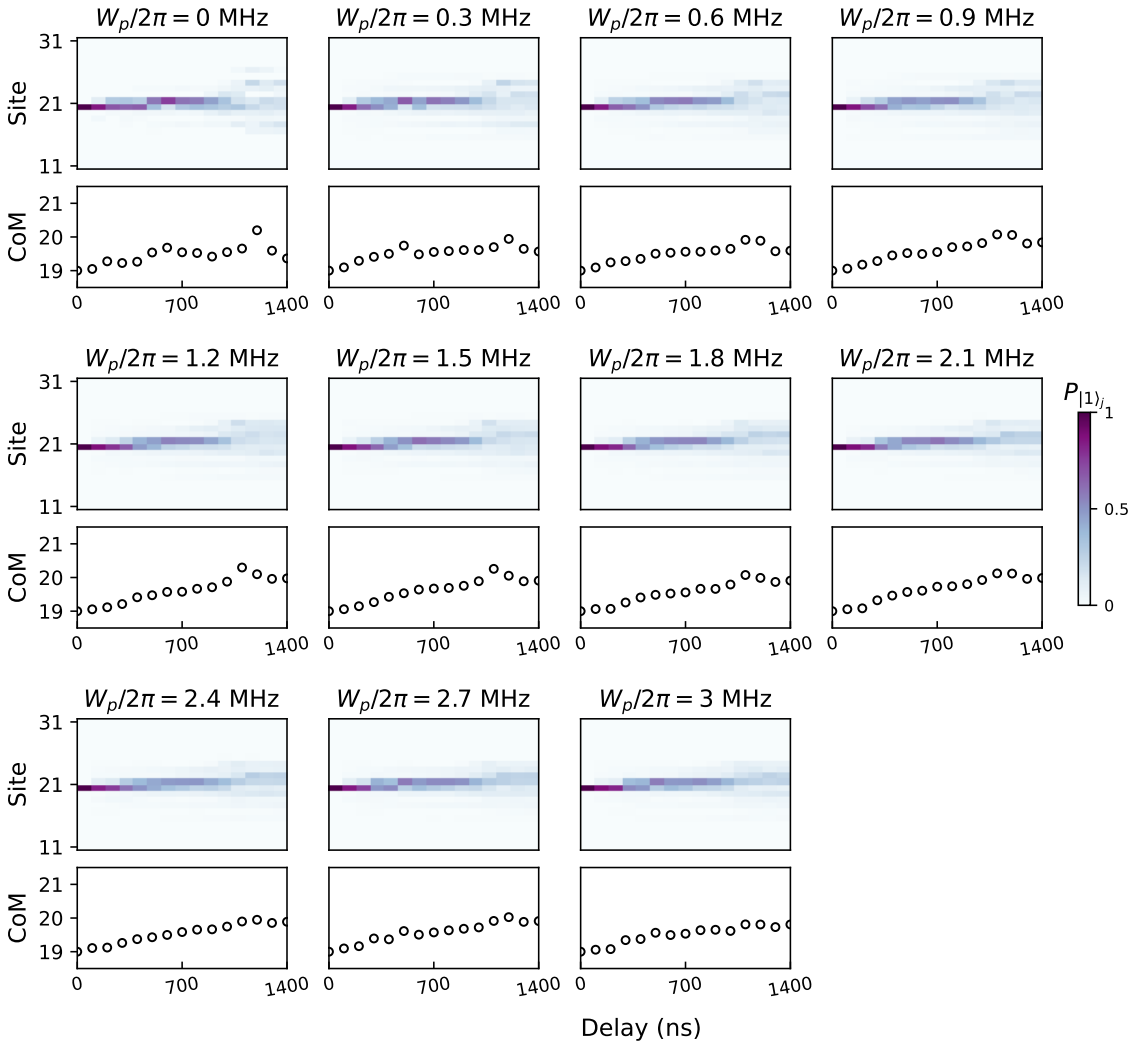

Supplementary Fig. 16. Experimental data of time evolutions of excitation probabilities and CoMs of pumping for single-loop trajectory $\mathcal{C}_{\rm sl}$ versus the disorder strength W_p. As the disorder strength increases, CoM moves as the delay increase, which *implies the existence of topological pumping induced by the quasi-periodic hopping disorder* [8].

Experimental Data Table for Supplementary Figure 12		
$V/2\pi$ (MHz)	δx	standard error
0	1.9563	0
4	1.8107	0.0337
8	1.6136	0.0461
12	1.3985	0.1025
16	1.2552	0.135
20	0.3771	0.1591
24	0.347	0.1388
28	0.117	0.1215
32	0.2668	0.1077
36	0.2116	0.1018

Experimental Data Table for Supplementary Figure 14		
$W/2\pi$ (MHz)	δx	standard error
0	1.9618	0.0
0.4	2.0358	0.0638
0.8	1.8591	0.1424
1.2	1.3807	0.205
1.6	1.0548	0.1720
2.0	1.0032	0.1651
2.4	0.5021	0.0871
2.8	0.3550	0.1803
3.2	0.1889	0.2364
3.6	0.3014	0.2462

Experimental Data Table for Supplementary Figure 15		
$V/2\pi$ (MHz)	δx	standard error
0	0.0406	0.0
2	0.2924	0.04995
4	0.4992	0.0575
6	0.5061	0.0814
8	0.6636	0.0907
10	0.7923	0.1037
12	0.7073	0.0683
14	0.8553	0.087
16	0.7256	0.1049
18	0.8147	0.1044
20	0.6323	0.0967
22	0.5447	0.1505
24	0.1554	0.1144
26	0.1501	0.1072
28	0.0888	0.1227

Experimental Data Table for Supplementary Figure 16		
$W_p/2\pi$ (MHz)	δx	standard error
0.0	0.3632	0.0
0.3	0.5683	0.0737
0.6	0.5936	0.115
0.9	0.8392	0.1007
1.2	0.9743	0.1674
1.5	0.9062	0.1531
1.8	0.9075	0.1585
2.1	0.9852	0.1538
2.4	0.8888	0.1569
2.7	0.91	0.0935
3.0	0.8095	0.1171

[1] Y.-H. Shi, Y. Liu, Y.-R. Zhang, Z. Xiang, K. Huang, T. Liu, Y.-Y. Wang, J.-C. Zhang, C.-L. Deng, G.-H. Liang, Z.-Y. Mei, H. Li, T.-M. Li, W.-G. Ma, H.-T. Liu, C.-T. Chen, T. Liu, Y. Tian, X. Song, S. P. Zhao, K. Xu, D. Zheng, F. Nori, and H. Fan, Quantum simulation of topological zero modes on a 41-qubit superconducting processor, Phys. Rev. Lett. **131**, 080401 (2023).
[2] D. J. Thouless, Quantization of particle transport, Phys. Rev. B **27**, 6083 (1983).
[3] D. Xiao, M.-C. Chang, and Q. Niu, Berry phase effects on electronic properties, Rev. Mod. Phys. **82**, 1959 (2010).
[4] R. Citro and M. Aidelsburger, Thouless pumping and topology, Nat. Rev. Phys. **5**, 87 (2023).
[5] M. J. Rice and E. J. Mele, Elementary Excitations of a Linearly Conjugated Diatomic Polymer, Phys. Rev. Lett. **49**, 1455 (1982).
[6] W. P. Su, J. R. Schrieffer, and A. J. Heeger, Solitons in Polyacetylene, Phys. Rev. Lett. **42**, 1698 (1979).
[7] M. M. Wauters, A. Russomanno, R. Citro, G. E. Santoro, and L. Privitera, Localization, Topology, and Quantized Transport in Disordered Floquet Systems, Phys. Rev. Lett. **123**, 266601 (2019).
[8] Y.-P. Wu, L.-Z. Tang, G.-Q. Zhang, and D.-W. Zhang, Quantized topological Anderson-Thouless pump, Phys. Rev. A **106**, L051301 (2022).
[9] R. D. King-Smith and D. Vanderbilt, Theory of polarization of crystalline solids, Phys. Rev. B **47**, 1651 (1993).
[10] N. Marzari, A. A. Mostofi, J. R. Yates, I. Souza, and D. Vanderbilt, Maximally localized Wannier functions: Theory and applications, Rev. Mod. Phys. **84**, 1419 (2012).
[11] N. Marzari and D. Vanderbilt, Maximally localized generalized Wannier functions for composite energy bands, Phys. Rev. B **56**, 12847 (1997).
[12] A. Cerjan, M. Wang, S. Huang, K. P. Chen, and M. C. Rechtsman, Thouless pumping in disordered photonic systems, Light Sci Appl **9**, 178 (2020).
[13] S. Nakajima, T. Tomita, S. Taie, T. Ichinose, H. Ozawa, L. Wang, M. Troyer, and Y. Takahashi, Topological Thouless pumping of ultracold fermions, Nat. Phys. **12**, 296 (2016).
[14] M. Lohse, C. Schweizer, O. Zilberberg, M. Aidelsburger, and I. Bloch, A Thouless quantum pump with ultracold bosonic atoms in an optical superlattice, Nat. Phys. **12**, 350 (2016).
[15] Y. Ke, X. Qin, Y. S. Kivshar, and C. Lee, Multiparticle wannier states and thouless pumping of interacting bosons, Phys. Rev. A **95**, 063630 (2017).
[16] P. W. Anderson, Absence of Diffusion in Certain Random Lattices, Phys. Rev. **109**, 1492 (1958).
[17] A. Anirban, 15 years of topological insulators, Nat. Rev. Phys. **5**, 267 (2023).
[18] G. Theodorou and M. H. Cohen, Extended states in a one-demensional system with off-diagonal disorder, Phys. Rev. B **13**, 4597 (1976).
[19] L. Fleishman and D. C. Licciardello, Fluctuations and localization in one dimension, J. Phys. C: Solid State Phys. **10**, L125 (1977).
[20] C. M. Soukoulis and E. N. Economou, Off-diagonal disorder in one-dimensional systems, Phys. Rev. B **24**, 5698 (1981).
[21] S. Nakajima, N. Takei, K. Sakuma, Y. Kuno, P. Marra, and Y. Takahashi, Competition and interplay between topology and quasi-periodic disorder in Thouless pumping of ultracold atoms, Nat. Phys. **17**, 844 (2021).
[22] S. K. Zhao, Z.-Y. Ge, Z. Xiang, G. M. Xue, H. S. Yan, Z. T. Wang, Z. Wang, H. K. Xu, F. F. Su, Z. H. Yang, H. Zhang, Y.-R. Zhang, X.-Y. Guo, K. Xu, Y. Tian, H. F. Yu, D. N. Zheng, H. Fan, and S. P. Zhao, Probing operator spreading via Floquet engineering in a superconducting circuit, Phys. Rev.

Lett. **129**, 160602 (2022).

[23] R. J. Marks, *Introduction to Shannon Sampling and Interpolation Theory*, Springer Texts in Electrical Engineering (Springer New York, 1991).

[24] K. Xu, J.-J. Chen, Y. Zeng, Y.-R. Zhang, C. Song, W. Liu, Q. Guo, P. Zhang, D. Xu, H. Deng, K. Huang, H. Wang, X. Zhu, D. Zheng, and H. Fan, Emulating many-body localization with a superconducting quantum processor, Phys. Rev. Lett. **120**, 050507 (2018).

[25] Q. Guo, C. Cheng, Z.-H. Sun, Z. Song, H. Li, Z. Wang, W. Ren, H. Dong, D. Zheng, Y.-R. Zhang, R. Mondaini, H. Fan, and H. Wang, Observation of energy-resolved many-body localization, Nat. Phys. **17**, 234 (2021).

[26] Z. Yan, Y.-R. Zhang, M. Gong, Y. Wu, Y. Zheng, S. Li, C. Wang, F. Liang, J. Lin, Y. Xu, C. Guo, L. Sun, C.-Z. Peng, K. Xia, H. Deng, H. Rong, J. Q. You, F. Nori, H. Fan, X. Zhu, and J.-W. Pan, Strongly correlated quantum walks with a 12-qubit superconducting processor, Science **364**, 753 (2019).